Stratification effect on the extreme-scale rolls in the plane Couette flows

Sergio Gandía-Barberá, Francisco Alcántara-Ávila, and Sergio Hoyas*
Instituto Universitario de Matemática Pura y Aplicada,
Universitat Politècnica de València, València, Spain

Victor Avsarkisov
Leibniz-Institute of Atmospheric Physics, Rostock University, Kühlungsborn, Germany
(Dated: February 22, 2021)

The existence of the large-scale structures appearing in turbulent Couette flows are studied by means of a new DNS dataset of active thermal Couette flows for different friction Richardson numbers, at the Prandtl number of air, Pr = 0.71. The existence of these structures is linked to the nonexistence of an active thermal flow. As soon the Richardson number is greater than 1.5, the structures are less energetic, and for a value of only 3, the structures have vanished. This is due to the reorganization of the intense Reynolds stress events. Thus, large-scale structures will hardly appear in real-life Couette flows of air with a stable wall-normal gradient of temperature.

I. INTRODUCTION

Turbulent channel flows have been widely studied for their relatively simplicity as a framework to study wall turbulence. The main control parameter is the friction Reynolds number, $Re_\tau = u_\tau h/\nu$, where u_τ is the friction velocity, h is the semi height of the channel and ν is the kinematic viscosity. Two different boundary conditions are usually imposed, pressure driven (Poiseuille, P-flows) [1–5] and shear (Couette, C-flows) [6–8] flows. Turbulent C-flows have been studied less and at lower Reynolds number than P-flows due to the existence of very large-scale roll-like motions extending along the streamwise and wall-normal directions of the domain. These large coherent structures were found experimentally [9–11] and numerically [7, 8, 12] in unstratified Couette flows. They are defined as coherent regions of either low or high streamwise velocity, creating counter-rotating vortex pairs almost aligned in the streamwise direction [12]. There is not a clear criterion to identify these structures. In ducts, these structures has been identified using threshold functions [13] but this has still to be done in Couette flows. They are mostly identified through visualization employing some filtering [7, 12].

The rolls are in fact quite stable. Kraheberger et al. [14] found that the rolls were not completely nullified by transpiration flows up to $Re_\tau = 1000$. Gandía-Barberá et al. [15] linked the existence of the rolls to only negative values on the one-point statistics of Reynolds stress in transitionary Couette-Poiseuille flows. Lee and Moser [12] found out that, up to $350h$ at $Re_\tau = 500$, the streamwise length of the rolls increases with the friction Reynolds number. Beyond this Reynolds number, it can be considered as infinite for all practical purposes. Finally, Alcántara-Ávila et al. [16] found that the width of the numerical or experimental domain has an important effect in the number and width of the rolls and, more important, in the one-point statistics of the flow.

The main idea of this study is to destabilize the counter-rotating rolls introducing an active thermal field, which causes a density stratification in the flow. The effect of stratification on rolls in the plane Couette flow is relatively less studied. However, it is well known that even the weak stratification can affect the Taylor-Couette flow and induce thin layering on the flow, not related to the Taylor vortex rolls [17]. On the other hand, there are some indications that even in the weakly stratified plane Couette flow at high Re_τ, coherent structures, and the near-wall turbulence regeneration cycle may be affected by the vertical stratification [18, 19]. Perhaps, one candidate for this phenomenon could be a rare cloud formation called the Morning Glory cloud, [20]. However, due to certain limitations in the atmospheric measurements techniques and spatial coverage, this comparison requires more observational and numerical efforts. Anyway, the results of the present analysis are relevant to the stratified turbulence in the atmosphere, as it is found at a large variety of stratification rates and Reynolds numbers [21].

II. METHODOLOGY AND NUMERICAL SIMULATIONS

The streamwise, wall-normal and spanwise coordinates are respectively denoted by x, y and z, and the corresponding velocity components are U, V and W. Density is denoted by ρ_t. Statistically averaged quantities are denoted by an overbar, whereas fluctuating quantities are denoted by lowercase letters, i. e. $U = \overline{U} + u$. There is one exception to this rule. As capital ρ is indistinguishable to P we have used a t subindex, $\rho_t = \overline{\rho} + \rho$. The superscript $(+)$ indicates that the quantities have been normalized by u_τ. Quantities averaged in time or in a particular direction are denoted using angles; that is, $\langle U \rangle_{xzt}$ for the streamwise velocity averaged in homogeneous directions and time.

The governing equations of the system are the Navier

* Corresponding author: serhocal@mot.upv.es

Case	Line	Re_b	Re_τ	Ri_τ	Tu_τ/h	TU_b/L_x
P0	———	10200	500	0	48.11	34.19
C0	·····	10500	480	0	41.96	33.03
C1	– – – –	10700	476	0.50	54.74	44.26
C3	—·—	11300	483	1.65	34.98	29.43
C6	———	11480	476	2.90	31.51	27.33

Table I: Parameters of the simulations. Two different Reynolds numbers are given depending on the bulk velocity, U_b, and u_τ. Ri_τ is given in the fifth column. The last two columns denote the computational time span while statistics were taken in wash-outs (U_b/L_x) and eddy turn-overs (u_τ/h). Line shapes are used to identify the cases through all the figures.

Stokes equations under the Boussinesq aproximation,

$$\partial_j U_j = 0, \tag{1}$$

$$\partial_t U_i + U_j \partial_j U_i = -\partial_i P + \frac{1}{\mathrm{Re}_\tau}\partial_{jj} U_i - \mathrm{Ri}_\tau \rho_t \delta_{i2}, \tag{2}$$

$$\partial_t \rho_t + U_j \partial_j \rho_t = \frac{1}{\mathrm{Re}_\tau \mathrm{Pr}}\partial_{jj}\rho_t. \tag{3}$$

In these equations Ri_τ is the Richardson friction number, given by $Ri_\tau = \Delta\rho g h/\rho_0 u_\tau^2$. This $\Delta\rho$ is the difference in density between the two walls, being the flow denser at the bottom wall. Thus, Dirichlet boundary conditions are used to model ρ_t. g is the gravitational acceleration and ρ_0 is a reference density. The Prandtl number of air is used in this study, $\mathrm{Pr} = 0.71$. The previous equations are transformed into an equation for the wall-normal vorticity ω_y and for the Laplacian of the wall-normal velocity $\phi = \nabla^2 v$. The spatial discretization uses dealiased Fourier expansions in x and z, and seven-point compact finite differences in y, with fourth-order consistency and extended spectral-like resolution [22]. The temporal discretization is a third-order semi-implicit Runge-Kutta scheme [23]. The code used for this work has been employed in different works for several different boundary conditions, [2, 7, 14, 24–26].

Five new simulations have been made for this work, summarised in Table I. The first simulation is a P-flow with $\mathrm{Ri}_\tau = 0$. The other four simulations are C-flows at different small values of Ri_τ. In every case, the domain chosen is $(8\pi h, 2h, 3\pi h)$, to completely contain a pair of rolls [16]. The mesh has a size of $(1536, 251, 1152)$ points which gives a resolution of 8.2 and 4.1 wall units in x and z. The wall-normal grid spacing is adjusted to keep the resolution at $\Delta y = 1.5\eta$, i.e., approximately constant in terms of the local isotropic Kolmogorov scale $\eta = (\nu^3/\epsilon)^{1/4}$. In wall units, Δy^+ varies from 0.83 at the wall, up to $\Delta y^+ \simeq 2.3$ at the centreline. This grid size is similar to the one typically used in channel flows, for both P- and C- Flows [2, 7, 12, 26].

In every simulation case, the flow had to evolve from an initial field, which has been taken from a previous case with lower Ri_τ. The code was run until a transition phase was passed and the flow had adjusted to the new set of parameters. The transition is characterized through, among other variables, the value of the shear stress in the moving wall. Once this parameter reaches a plateau, statistics are collected as in [19, 27]. In order to further validate the database, the total density flux, which is equal to one, has been calculated as the sum of the turbulent and molecular density fluxes. The following equation comes from integration of Eq. 3,

$$1 = \overline{v\rho}^+ - \frac{d\overline{\rho_t}^+}{dy^+}, \tag{4}$$

and it is shown in Figure 1. All fluxes collapse perfectly, and in every case their sum is one, with an error below 5×10^{-3}.

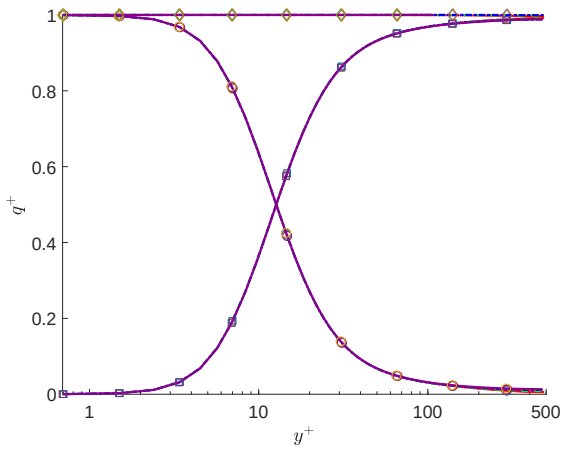

Figure 1: Colour online. Turbulent (squares), molecular (circles), and total (diamonds) density fluxes for cases C0, C1, C3 and C6. The collapsing of the different curves is perfect.

III. RESULTS AND DISCUSSION

A. Stratification on velocity fields

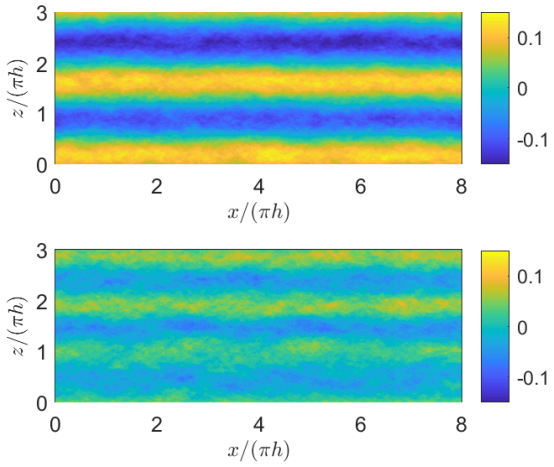

Figure 2: Colour online. X-Z plane at the center of the channel of $\langle u/U_b \rangle_t$ for the cases C0 (top) and C6 (bottom).

Isosurfaces of u/U_b are plotted at the channel centre for cases C0 and C6 in Figure 2. The streamwise streaks in case C0 are trackers of the large-scale rolls [12, 15]. Streaks and rolls are involved in a regeneration cycle (i.e. self-sustaining mechanism) in both the buffer [28] and the logarithmic layer [29]. In this process, a streak flanked by an attached Q2 and Q4 event occasionally meanders and destroys itself generating a peak of wall-normal velocity, Reynolds stress and dissipation. This fact is observed in the intermittent bursts of logarithmic wall-attached events. The bursting process reinforces the rolls, which eventually eject low-speed fluid from the wall creating streamwise streaks through a lift-up process [31]. While these rolls are strong and clearly defined for C0, their strength and definition is reduced in C6 due to stratification. This can be seen in Figure 3, where $\langle u(y/h = 1)/U_b \rangle_{tx}$ is shown for the four cases. While C0 and C1 present four extrema, corresponding to the yellow (fast) and blue (slow) streaks of Figure 2 top, C3 and C6 present six weaker peaks. The disruption of the self-sustaining mechanism by a stable stratification in channel Couette flows was predicted by Eaves and Caulfield [18] by observing the laminar to turbulent transition of neutral and stratified cases. Stable stratification damps turbulent wall-normal motions by imposing a potential energy toll [27]. This feature disrupts the well-established self-sustaining mechanism by modifying the energy input into rolls and consequently reducing the kinetic energy density of the streaks. The level of disruption increases with the bulk Richardson number, Ri_B. The authors observe that the disruption is significant at a Richardson bulk number $Ri_B \geq 3 \times 10^{-3}$. In our study,

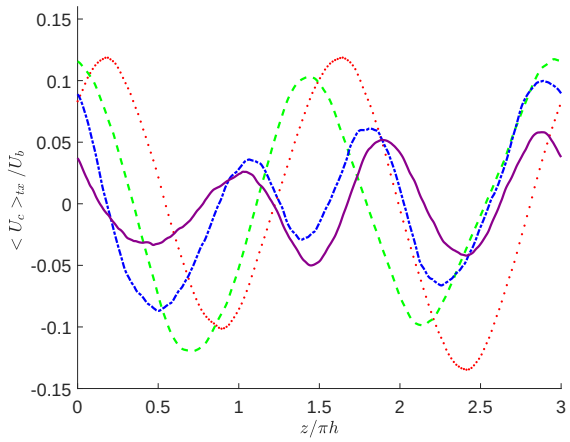

Figure 3: Colour online. Lines as in Table I. $\langle u/U_b \rangle_{xt}$ at the center of the channel represented along the spanwise direction.

the case C6 has $Ri_B = 1.2 \times 10^{-2}$.

More information about the 3D shape of the rolls can be obtained from the spectral density, $\Phi = k_x k_z E(k_x, k_z)$, where k_x and k_z are wave numbers in their sub-index direction and $E(k_x, k_z)$ is the energy spectrum of u. They are presented in Figure 4. The four figures have been plotted using the same scale to highlight the range in the energy from the largest scales to shorter ones. The black lines correspond to case P0. The two rolls in C0 and C1 are identified by the energy spectrum peak at $\lambda_z/h = 3\pi/2 = 4.7$ in the channel center. The same wavelength was identified in [15] for unstratified Couette at $Re_\tau = 125$, which indicates that rolls in $Re_\tau = 480$ have the same width; that is, $3\pi h/4 \approx 2.4h$. Even if Figure 3 can give the impression that the rolls in C6 are present but only in more quantity and less energetic, we can see in Figure 4 that in C6 they have disappeared for $y^+ < 100$. Additionally, their width has reduced. Near-wall structures are also identified in Figure 4 at $y^+ = 10$ at both walls. This region is mainly dominated by coherent streaks of streamwise velocity with an average spanwise separation of the order $\lambda_z^+ \approx 100$ [1].

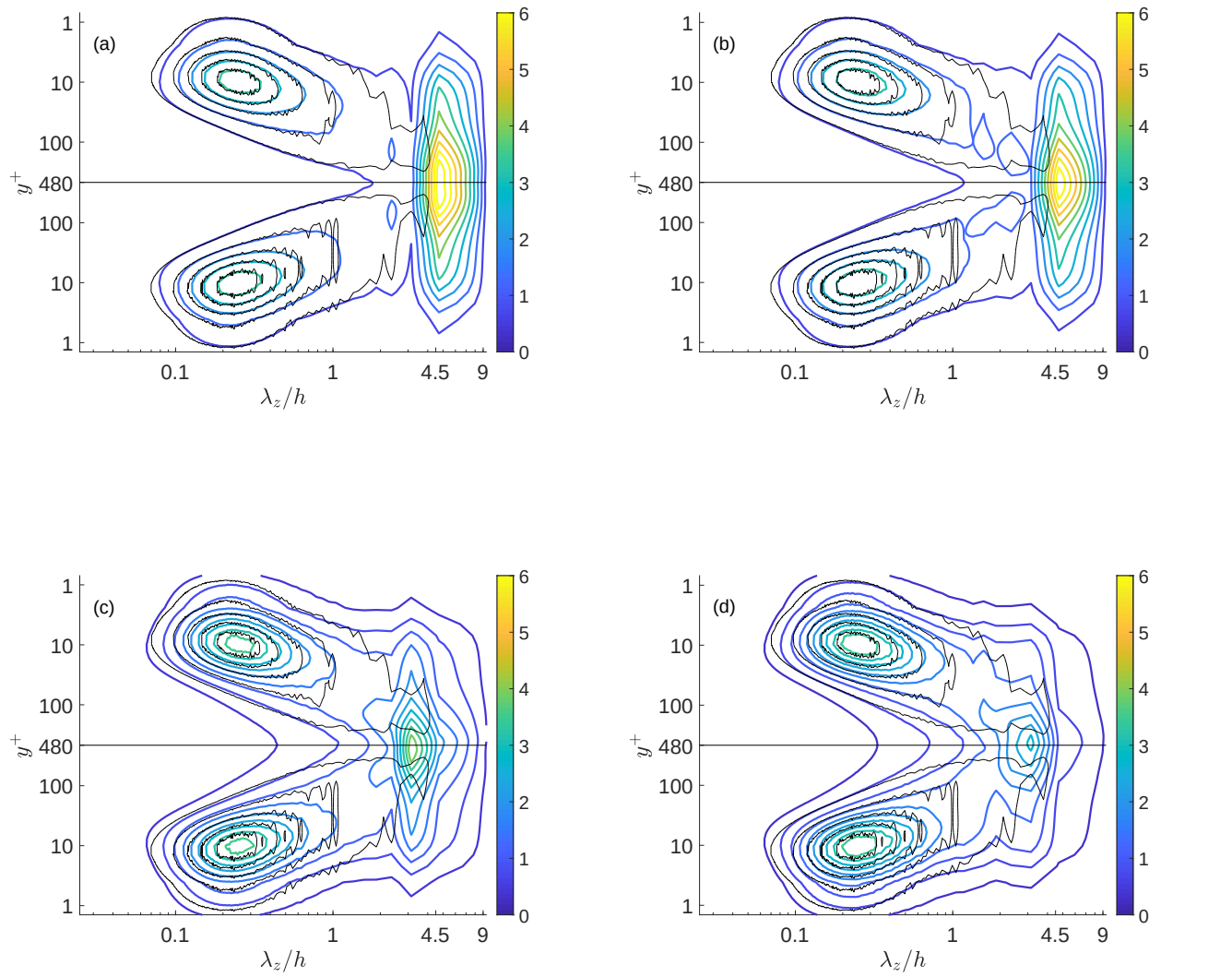

Figure 4: Colour online. Time- and x-averaged images of u/U_b at $y = h$ for cases C0, C1, C3 and C6 ((a) to (d)). In all cases the black lines correspond to case P0.

Thus, increasing Ri_τ causes the break-up of the rms-averaged rolls by weakening the streaks in the channel center as observed in Figure 2. However, other quantities such as the turbulent heat flux $\overline{v\rho}^+$ and the Reynolds stress $\overline{uv}^+$ (not shown here) do not change for the range of stratification (i.e. Ri_τ) achieved in this article. The reason that both quantities are unaffected can be linked to the close relationship between the velocity and the temperature fields. Deusebio et al. [19] indicates that the Reynolds stress and the turbulent heat flux decrease proportionally with stratification, so their ratio remains close to constant. Moreover, Garcia-Villalba [27] shows that a deviation of the Reynolds stress in a stratified turbulent channel at $Re_\tau = 550$ is only appreciable from $Ri_\tau \geq 60$. Thus, changes in these averaged quantities shall not be expected at $Ri_\tau < 3$.

B. Coherent structures of intense Reynolds stress

As a consequence of the self-sustaining mechanism, coherent structures in the form of counter-rotating rolls are triggered by pairs of ejections and sweeps extending beyond the buffer layer in a well-organised process called bursting. The ejections carry low streamwise velocity upwards from the wall ($u < 0$, $v > 0$), while

the sweeps carry high streamwise velocity downwards to the wall ($u > 0$, $v < 0$). Based on a Reynolds stress quadrant classification, ejections and sweeps are Q2 and Q4 events, respectively. Lozano-Duran et al. [30] and Jiménez [31] reported the relation between counter-rotating rolls, streamwise streaks and Q2-Q4 pairs in turbulent Poiseuille flow by observing averaged flow fields conditioned to the presence of a wall-attached Q2-Q4 pair. A wall-attached event is an intense Reynolds stress structure (i.e. uv-structure) that approaches a wall below $y^+ < 20$. The reasoning for this definition is explained later. For a time-resolved view of the bursting process in turbulent Poiseuille channel at $Re_\tau \approx 4200$, the interested reader is referred to [32].

In order to study the underlying mechanics behind the counter-rotating rolls, the coherent structures responsible for the transport of momentum are analysed. Jiménez [31] explains that the intensity of a given parameter is considered as an indicator of coherence, among other characteristics. However, the selection of a threshold is only feasible if the parameter is intermittent enough to separate between high- and low-intensity regions. After analysing the intermittency of different parameters, it is found that quadratic parameters, specially the Reynolds stress, are more appropriate to describe intense coherent structures.

Based on the above-mentioned evidence and the link between rolls and $\overline{uv}^+$ [15], a quadrant study of the flow through the intense Reynolds stress events was carried out following the identification method proposed in Lozano-Duran et al. [30]. A uv-structure is defined by connecting points in the flow field grid that satisfy:

$$|\tau\left(\vec{x},t\right)| > H u'_{rms}\left(y\right) v'_{rms}\left(y\right) \tag{5}$$

where $\tau\left(\vec{x},t\right) = -u'\left(\vec{x},t\right) v'\left(\vec{x},t\right)$ and H is the percolation index, discussed later.

The structure connectivity is defined in the 26 orthogonal directions of the DNS Cartesian mesh. The average streamwise and wall-normal component of each connected structure (i.e. domain Ω) is calculated following Eq. 6. Each uv-structure is classified in a given uv-quadrant from Q1 to Q4 based on the sign of its u'_m and v'_m.

$$u'_m = \frac{\int_\Omega u'\, dV}{\int_\Omega dV} \tag{6}$$

the same definition is used for v'_m.

Note that this approach for the average velocity components can be easily computed by considering that each structure point is located inside a small box of same size as the field grid at that point. Inside the box, the velocity value is constant and equal to the value at the point. This small box is from now referred as voxel, based on the definition in [33]. The voxel streamwise and spanwise dimensions remain constant at 8.2 and 4.1 wall units respectively, while the wall-normal dimension depends on its distance to the nearest wall.

Following the indications in [30], the sign of v'_m is changed on the structures at the upper channel half in Poiseuille flow. On turbulent Couette flow the sign of u'_m must be changed in this region, too. The reasoning is the same in both cases, the change on sign allows connected Q2 ($u < 0$, $v > 0$) and Q4 ($u > 0$, $v < 0$) events to extend beyond the central plane. Without these modifications, their part crossing the central plane would be wrongly considered as Q1 and Q3 points.

Various authors [34, 35] have pointed out the need of a wall-dependent threshold in non-homogeneous flows such as channel domains. If the threshold in Eq. 5 were evaluated in the buffer layer, the filter would barely identify structures in the logarithmic and outer regions. On the contrary, a threshold evaluated above the buffer layer would identify too many points near the wall, which would be falsely clustered into one huge uv-structure. The selection of a percolation index (H), independent of the wall distance, is based on the ratio of identified structures at a given H to the maximum number of objects among all studied indexes, $N(H_k)/max(N(H))$, being $k = 1, ..., n$ studied indexes; together with the ratio between the largest volume and the total volume identified at each index, $max(V(H_k))/sum(V(H_k))$. Figure 5 depicts the evolution of both parameters. The percolation study shows how the identified uv-structures cluster into a huge unique structure at $H < 1.5$, since the volume ratio is near 1. On the contrary, disperse structures of few volume units are identified from $H > 3$, being the volume ratio below 10^{-1}. Notice that such high percolation indexes identify less structures because the threshold (Eq. 5) is more restrictive. A similar behaviour was reported in [30, 36] for neutral turbulent Poiseuille at $Re_\tau = 934$ and $Re_\tau = 2003$.

From our understanding, this is the first time a percolation study for the identification of intense uv-events is done on a turbulent Couette flow, either neutral or stratified. Based on the results in Figure 5, the percolation index for C0 is 2.3. H is generally selected in the region after the percolation crisis (i.e. decay of volume ratio). For P0, H is 1.75 as in [30]. The percolation index for C6 is 2.1 in order to identify the same Reynolds stress as in C0, which is constant near -0.4 above the buffer layer, as will be seen later. Despite reducing the index in C6, the contributions of the uv-events to the total identified Reynolds stress remain the same as if $H = 2.3$ was set.

After applying the filtering in Eq. 5 with the selected percolation indexes, each uv-structure is assembled by the connectivity algorithm and engulfed in a box of dimensions $\Delta_x \times \Delta_y \times \Delta_z$ aligned to the Cartesian axes, where $\Delta_y = y_{max} - y_{min}$ and the same in the other directions. The limits of the box are defined by the first and last structure point in a given direction. The distances y_{min} and y_{max} to the nearest wall are relevant due to the inhomogeneity of the flow in the wall-normal direction.

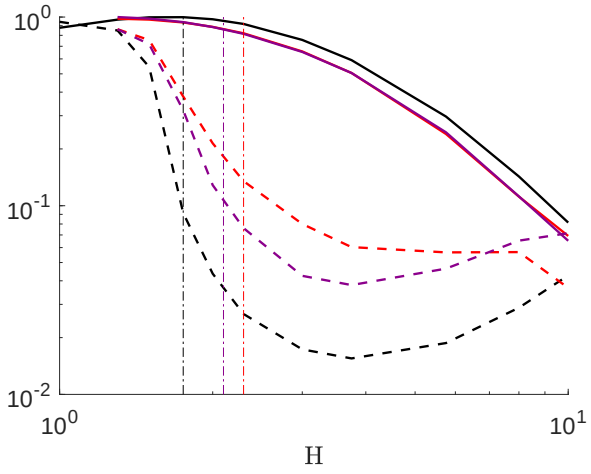

Figure 5: Colour online. Lines as in Table I. Percolation study for the identification of intense uv-structures. The solid lines are the ratio of identified objects to the maximum of objects identified among the studied percolation indexes. The dashed lines are the ratio of the volume of the largest identified object to the total volume identified at a given percolation index. The vertical lines are at $H = 1.75$, $H = 2.1$ and $H = 2.3$.

Lozano-Duran et al. [30] and Osawa [36] showed through joint PDF plots of y_{min} and y_{max} that the uv-events can be classified into 2 groups: attached $\left(y^+_{min} < 20\right)$ and detached $\left(y^+_{min} \geq 20\right)$. The same classification has been proven true for the turbulent Couette cases. See Figure 6.

A summary of the identified events is compiled in Table II. Here, uv-structures with a volume below 16^3 wall units are discarded to avoid grid resolution issues. They are neither included in the table nor in the figures. The structures are classified in the table as attached or tall-attached structures $\left(y^+_{min} < 20,\, y^+_{max} > 100\right)$, reaching the logarithmic region of the flow. The remaining structures are therefore detached. Since our aim is to study the channel-centre counter-rotating rolls in Couette from the underlying bursting cycle (i.e. intense uv-events), we focus on tall and energetic structures that reach this region. Lozano-Duran et al. [30] found that structures extending beyond the buffer layer carry a great fraction of Reynolds stress, so they are perfect candidates to study the organization of momentum transfer. Finally, it is observed later in Figure 7 that the stratification affects mainly the intensity of events at $y^+ > 100$.

As expected from Figure 5, low percolation indexes identify more structures, so N_T increases in Table II. 78% of the identified uv-events are Q2 (i.e. ejections) and Q4 (i.e. sweeps) independently of the case. Attached Q2 and Q4 events account for the 40% of identified structures, while only 8% of N_T are tall-attached. Q1 and Q3 events (i.e. Q^+) account only for the 20% of events, but almost none of them ($< 1\%$) is attached. These structures are less frequent and smaller in volume than Q2 and Q4 events (i.e. Q^-). Note that Q^+ volume is only 8% of the total identified volume. It is surprising that the volume of tall-attached structures is around 80% of the total identified volume, despite the low percentage of tall-attached events. Finally, despite 62% of the uv-events are detached, they contain only a 20% of the identified volume. At a first glance, it is not possible to find differences in Table II between cases P0, C0 and C6. These results agree with Jiménez [31], who points out that Q^+ events are small in Poiseuille channels and in homogeneous shear turbulent flows too. An explanation for the imbalance of structure types is that Q^- events ($u'v' < 0$) extract energy from the shear, while Q^+ events ($u'v' > 0$) lose it. Consequently, Q^- events tend to grow, with some individuals reaching the domain walls and developing attached structures, while Q^- events tend to vanish.

The turbulent momentum flux conditioned to uv-events is represented in Figure 7 along the wall-normal direction. The use of an identification threshold dependent on the wall distance results in a constant total identified Reynolds stress for C-flows and constant quadrant contributions away from the wall in all cases. Note that by employing a slightly lower percolation index at C6 the same amount of total Reynolds stress as in C0 is gathered by the filter. The quadrant contributions in P0 agree well with the results in [30] for turbulent channels at $Re_\tau = 934$ and $Re_\tau = 2003$. However, in our study the distortion in the statistics of quadrant contributions is visible near the channel center from $y^+ > 464$ ($y/h > 0.93$), only in P-flows.

Despite the overall Reynolds stress does not change with stratification up to $Ri_\tau \approx 3$, Figure 7 shows that the intensity of uv-structures is redistributed mainly between attached Q2 and Q4 events from $y^+ > 20$. The stratification up to $Ri_\tau = 3$ does not affect the organization of the Reynolds stress below this height. García-Villalba [27] noticed that turbulence under weak stratification ($Ri_\tau \leq 24$) is affected by buoyancy far from the wall, but the near-wall region differs little from the neutral case.

In C0 attached Q2 events (Figure 7, top), achieve a constant Reynolds stress from $y^+ > 40$ twice as intense as the Q4 events. In fact, from $y^+ > 100$ attached Q^- events contain almost 90% of the filtered Reynolds stress. In C6 although perfect collapse with C0 is lost from $y^+ > 20$, the same trend in Reynolds stress distribution is followed until $y^+ = 40$. Above this height, attached Q2 events carry less shear intensity while being redistributed to Q4 events, which keeps the overall Reynolds stress unchanged. At the first glance, it seems that attached Q4 events become more intense, but this is not true. Figure 9 shows that individual tall-attached Q4 events in average are less intense than tall-attached Q2, even under the effect of stratification. The reason for the reorganization in Figure 7 (top) is that there are more identified points of Q4 events extending beyond the buffer layer than Q2. This fact is observed in Figure 8 (bottom) and in the

Case	N_T	N_1	N_2	N_3	N_4	V_T	V_1	V_2	V_3	V_4
P0 (all)	12910	0.12	0.39	0.10	0.39	0.115	0.003	0.09	0.002	0.018
P0 (attached)	-	0.01	0.17	0	0.16	0.094	0.001	0.082	0	0.011
P0 (tall attached)	-	0.002	0.05	0	0.03	0.093	0.001	0.081	0	0.011
C0 (all)	5724	0.11	0.44	0.09	0.36	0.039	0.001	0.022	0.003	0.013
C0 (attached)	-	0.01	0.20	0	0.21	0.033	0.001	0.020	0.002	0.011
C0 (tall attached)	-	0	0.04	0	0.02	0.032	0.001	0.019	0.002	0.010
C6 (all)	7104	0.12	0.42	0.10	0.35	0.050	0.003	0.020	0.001	0.025
C6 (attached)	-	0.01	0.18	0	0.17	0.040	0.002	0.016	0.001	0.021
C6 (tall attached)	-	0	0.05	0	0.02	0.039	0.002	0.015	0.001	0.021

Table II: Time-averaged data of the identified intense uv-structures with $H = 1.75$ for P0, $H = 2.3$ for C0 and $H = 2.1$ for C6. N_T is the number of identified objects. N_i is the numerical fraction of objects classified in each uv-quadrant and in a given class (all, attached, tall-attached) among N_T. V_T is the numerical fraction of the total identified volume divided by the domain volume. V_i is the same fraction for each uv-quadrant. Attached structures have $y^+_{min} < 20$ and tall-attached structures have additionally $y^+_{max} > 100$. The remaining events are detached.

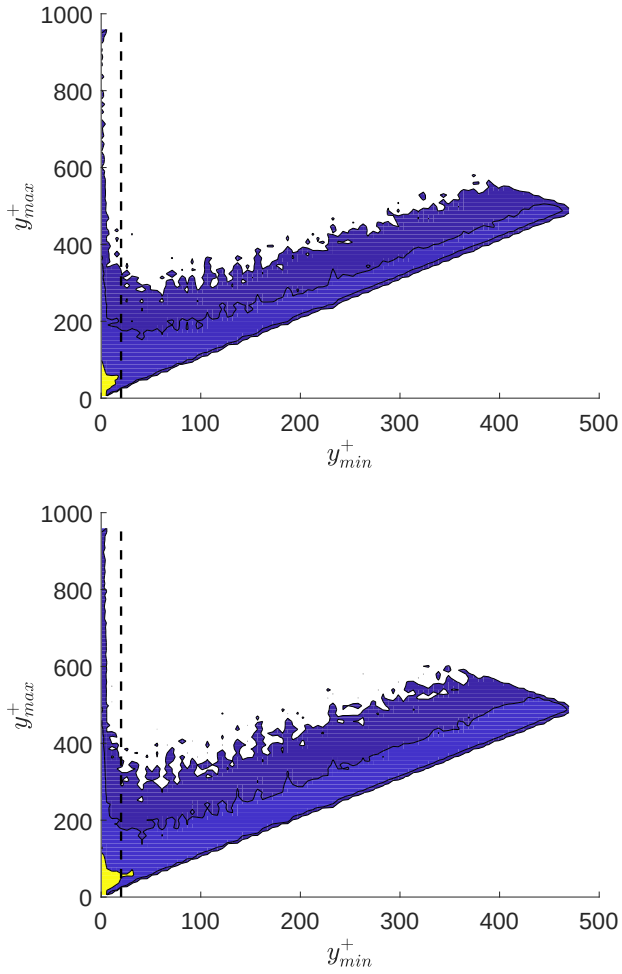

Figure 6: Joint PDF of the wall-normal distance to the closest domain wall from uv-structure bottom (y^+_{min}) and top (y^+_{max}). Figure on top is for C0 and below is for C6. Structures of all quadrants were considered in the plots. By definition, $y^+_{max} \geq y^+_{min}$. The vertical dashed line is located at $y^+_{min} = 20$. For each case, the plotted contours contain 40%, 90% and 98.8% of the total data.

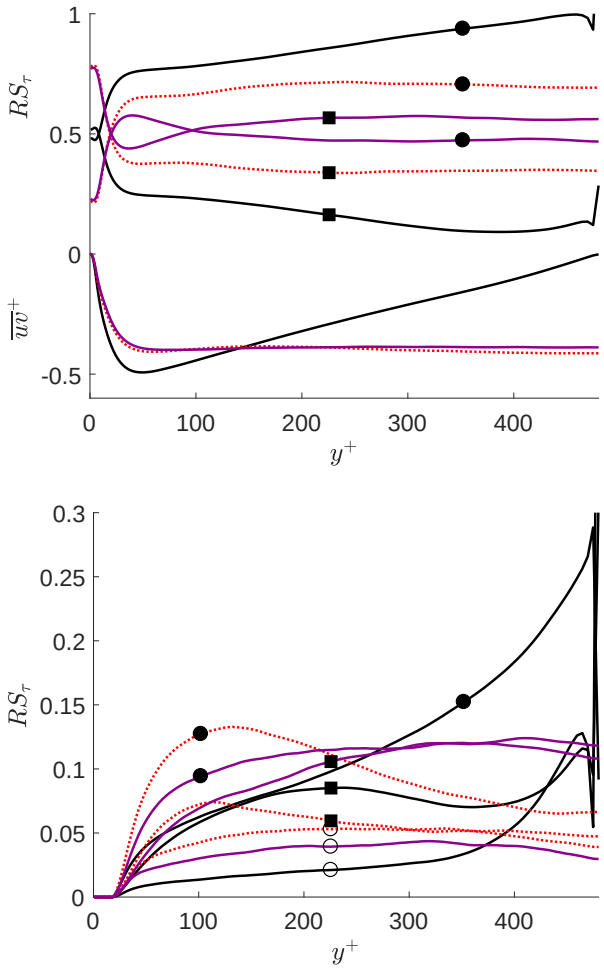

Figure 7: Colour online. Lines as in Table I. $\overline{uv}^+$ (figure on top, negative y-axis) is the Reynolds stress contained in the identified intense uv-events. RS_τ (positive y-axis) is the fraction of $\overline{uv}^+$ linked to: ●, Q2 events; ■, Q4 events; ○, Q^+ events. RS_τ in figure on top is for attached events, while in the figure below is for detached events.

volume of tall-attached events in C6 in Table II. Therefore, since the number of points linked to tall-attached Q4 events is higher in C6 than in C0, the contribution of this kind of uv-structure at $y^+ > 100$ increases. The reorganization in Reynolds stress away from the wall strengthen the relevance of the tall-attached structures in the study of stable stratification. Note that the Reynolds stress employed in Figure 7 is calculated at each identified point belonging to a uv-structure. Here the average velocities described in Eq. 6 are only used to classify each structure among the uv-quadrants.

By observing the Reynolds stress distribution among detached (Figure 7, bottom) events, the percentage of Q^- intensity in C0 due to detached events grows from 0% at $y^+ = 20$ (by definition) until 20% at $y^+ = 100$. This percentage is reduced linearly until 10% near the channel center, reflecting the relevance of tall-attached events in this region.

In C6 the contribution of detached Q^- events increases with the wall distance until reaching a 20% in the channel center. In this case the intensity of the detached events is greater than in neutral Couette. Finally, only 5% of the filtered Reynolds stress is carried by Q^+ events in all cases. The contribution of detached Q^+ tends to cancel the one of detached Q^- in C0, but this does not happen in C6. Lozano-Duran et al. [30] found that in Poiseuille flow detached events are isotropically oriented and scale in Kolmogorov units, so they can be considered dissipative objects in terms of momentum transfer. Additionally, in average the contribution of detached events cancel each other. Based on these evidences together with the high percentage of Reynolds stress carried by attached uv-structures, this study is focused on the latter. The higher percentage of Reynolds stress located in detached structures under stratification may stem from the damping of turbulent wall-normal motions, which reduces the average intensity ($\tau_m^+ = u_m^+ v_m^+$) in both attached (Figure 9) and detached (not shown here) structures. This reduction limits the growth of the structures born above the buffer layer, so less structures can reach a domain wall and become attached.

Stratification develops a completely different scenario far away from the wall with regard to the intense tall-attached Q events. Figure 8 (top) shows the spanwise distribution of the Reynolds stress averaged in the logarithmic and outer region of the channel. The most obvious result is that tall-attached Q^- events in C0 are perfectly organized spanwise with a constant spacing around $2.4h$. See in Figure 8 (bottom) that the points corresponding to tall-attached Q^- events follow the same organization as the uv-stress locations. In this figure, the greater $\langle N \rangle_{xt}$ is for a given kind of structure in a spanwise position, the higher this kind of structure grows in the wall-normal direction. Notice that the Reynolds stress, either Q2 or Q4, is clearly located in given spanwise regions and along the streamwise direction, leaving gaps with almost no momentum transport. This kind of information is unfortunately lost in Figure 7 due to the average in spanwise

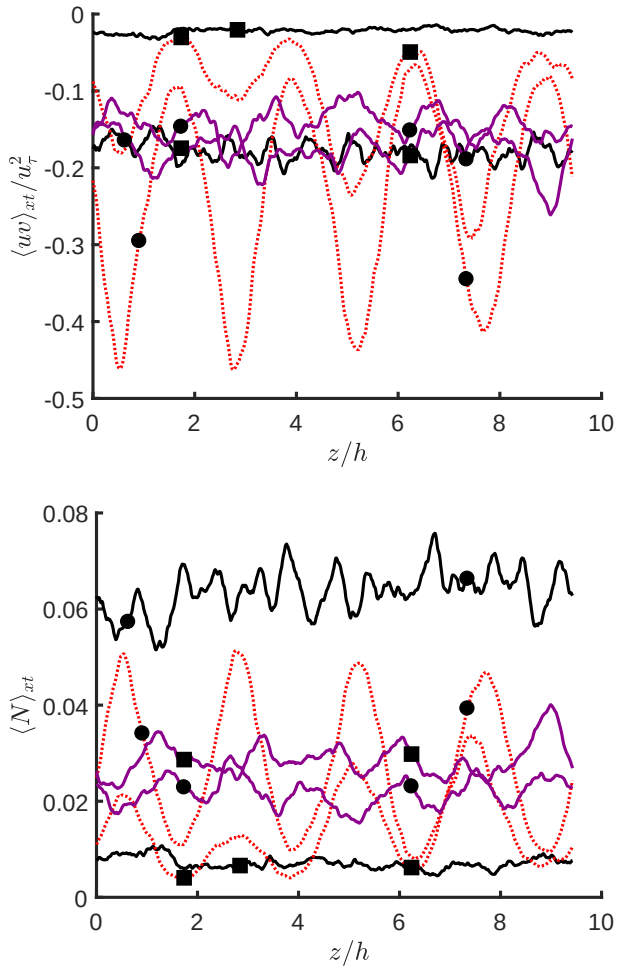

Figure 8: Colour online. Lines as in Table I. Markers as in Figure 7. Top: $\langle uv \rangle_{xt}/u_\tau^2$, Reynolds stress contained in the attached Q2 and Q4 events. Bottom: $\langle N \rangle_{xt}$ ratio of grid points corresponding to each uv-structure identified along the wall-normal direction above the buffer layer. The parameters are averaged in time, streamwise direction and in $100\,\nu/u_\tau \leq y \leq h$.

direction. This organization is explained by the position of the outer high- and low-speed streaks in neutral Couette. Gandia-Barbera et. al [15] showed that these streaks extend along the streamwise direction and have a constant spanwise spacing of $2.4h$, independently of Re_τ. Additionally, the authors illustrated that the streaks are located in zones of intense Reynolds stress in planes averaged in time and streamwise direction. As stated before, Q^- events are generally located on streamwise streaks. Q2s ($u'_m < 0$) are present in low-speed streaks and Q4s ($u'_m > 0$) in high-speed streaks. Due to the reduced streamwise length of the uv-structures (reported later in Figure 10) in comparison to the length of the streaks, it is considered that uv-structures are a consequence of the presence of the streak. Additionally, uv-structures are generated by the presence of shear rather than the

presence of a wall [31]. Linking all these facts, the spatial organization of counter-rotating rolls, streaks and uv-structures is understood for neutral Couette flow. The presence of large outer streaks influences the location of Q^- events, which can grow reaching $y^+_{max} > 100$ due to the strong shear stress (i.e. Reynolds stress) located in the streaks. Such intense Q^- events shown in Figure 8 generate in time-average clear counter-rotating rolls that reach both domain walls and extend almost infinitely in the streamwise direction [12]. However, the spanwise distance between outer streaks is still an open question.

The weakening of the streaks due to stratification in C6 (See Figure 4) develops a disorganized scenario since there are no preferential spanwise locations for the Q^- events. The Q^- points in Figure 8 (bottom) show a constant spanwise distribution, leading the Reynolds stress in Figure 8 (top) to be evenly distributed in the spanwise direction. The difference in uv-intensity between attached Q2 and Q4 at P0 is in accordance with the results in [30], who showed that attached Q4 are more intense near the wall and that most of the intense events reaching $y^+_{max} > 100$ are attached Q2 in Poiseuille channels. This fact is observed in the number of tall-attached Q2 points identified in comparison to Q4 points. Notice that in average in neutral cases (i.e. P0 and C0) tall-attached Q2 events grow higher than Q4 events, and the opposite occurs in the stratified case. This fact is related to the difference in Reynolds stress carried by each event. Figure 9 shows that generally tall-attached Q4 events are less energetic than tall-attached Q2. This is a well-known fact, already discussed in [30]. However, the intensity is reduced in C6 with stratification due to the restrictions on vertical motions. Attached Q^- events in stratified Couette flow (i.e. C6) are less energetic in terms of averaged Reynolds stress (τ^+_m) than in neutral Couette flow. The reduction has the same effect on both Q2 and Q4, that lose in average 28% of their intensity. Since these structures extract energy from the mean flow shear in order to grow, it is assumed that the amount of Reynolds stress carried is directly proportional to their growth. Nevertheless, the fact that in Figure 8 the tall-attached Q4 events grow higher and show a similar intensity as Q2 events may stem from the differences on the average techniques. In Figure 8 the average is calculated point-wise considering only the points above $y^+ > 100$ contained in attached events, however in Figure 9 (bottom) all the points contained in tall-attached events are averaged. This means that tall-attached Q4 events are more intense above the buffer layer than Q2 due to stratification, but when all the points contained in the structure are considered, tall-attached Q2 events are more intense in average than Q4 events.

The averaged Reynolds stress (τ^+_m) agrees roughly with the averaged vertical velocity ($v^{'+}_m$) as observed in Figure 9 (top). This fact is consistent with the mixing-length argument in which the Reynolds stress is generated by displacing the mean velocity profile by an amount proportional to the structure size. As a result, in the logarithmic layer $\tau^+ \approx 1/\kappa\, v^+ \propto v^+$ [30], being $\kappa \approx 0.4$ the Kármán constant.

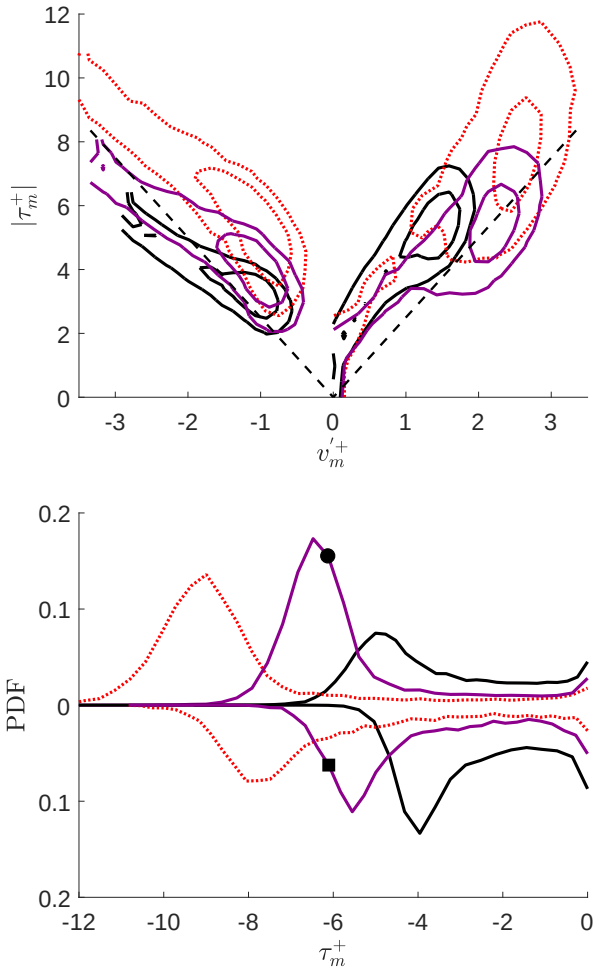

Figure 9: Colour online. Lines as in Table I. (Top) Joint PDF of the averaged wall-normal velocity $v^{'+}_m$ and the averaged Reynolds stress $\tau^+_m = u^{'+}_m \cdot v^{'+}_m$ of tall-attached Q2 ($v^{'+}_m > 0$) and tall-attached Q4 ($v^{'+}_m < 0$). Dashed lines are $\tau^+_m = \pm 2.5 v^{'+}_m$. For each case, the plotted contours contain 50% and 90% of the data. (Bottom) PDF of the averaged Reynolds stress for tall-attached Q2 and Q4 events above and below $PDF = 0$. Symbols as in Figure 7. The quantities are averaged following Equation 6.

Finally, notice in Figure 9 (top) that Q4 events are limited to a minimum $v^{'+}_m < 0$ due to the impermeability condition of the wall. Lozano-Duran et al. [32] states that a given structure does not need to be attached or detached over its full lifetime. Ejections (Q2) start their lives attached, move away from the wall, and eventually detached. Sweeps (Q4) behave the other way around, being limited by the wall as soon as they approach it.

Various authors have reported that intense attached structures of diverse parameters reaching the logarith-

mic region are self-similar. That is, the length (Δx) and width (Δz) of each object is proportional to the distance to the nearest wall ($y \approx \Delta y$ due to attached condition). Lozano-Durán [30] and Osawa [36] reported self-similar attached uv-structures in turbulent Poiseuille flow at $Re_\tau > 900$. Del Álamo et. al [34] reported this attribute on attached vortex clusters identified through the velocity gradient tensor $\nabla \mathbf{u}'$. Yoon et. al [37] declared the self-similarity of u-structures of intense streamwise velocity fluctuations in turbulent boundary layers subjected to an adverse pressure gradient. In our study the size of the boxes containing attached uv-structures reaching the logarithmic region are studied on turbulent neutral and stratified Couette channel and compared to turbulent neutral Poiseuille channel.

The joint PDF graphics of the dimensions of boxes containing attached Q^- events (Figure 10 (a) and (b) show three regions. In the near-wall region ($\Delta y^+ \leq 100$) there are differences between Q2 and Q4 events, despite the perfect collapse between neutral and stratified Couette. Q4 events get closer to the wall than Q2 events. This is expected because their negative v_m tends to flatten them against the domain wall. This fact occurs in Poiseuille flows too [30]. In the logarithmic and outer region ($\Delta y^+ > 100$) a good collapse between cases and Q^- events is found. This fact is ratified with the perfect collapse in the 1D PDF plots in Figure 10 (c) and (d). Notice that P0 is not depicted in the joint PDF plots for simplicity, although a perfect collapse is achieved in the logarithmic region as observed in the 1D PDF figures.

Finally, the third group is the attached Q^- events extending beyond the center line ($\Delta y^+ > Re_\tau$). These objects reach $\Delta x \approx 6.25h$ and $\Delta z \approx 2.08h$. Lozano-Durán [30] found that these events are juxtapositions of smaller objects gathered by the connection algorithm which do not agree with the self-similar ratios of other tall-attached objects. Additionally, this part of the joint PDF changes with small variations of percolation index around the selected value. All these features are found in our study too despite the difference in the directions of the connection algorithm. This region is more pronounced in length than in width, together with the fact that for a given Δy^+ the length has a greater range of values than the width. The length range is more sensitive to the friction Reynolds number than the width range when comparing our results at $Re_\tau = 480$ with Lozano-Durán [30] at $Re_\tau = 934$ and 2003. This fact reinforces the idea that the mechanisms that deform the structures along the two coordinates are different. The deformation along the streamwise direction is due to shear, while the background turbulence deforms the objects along the spanwise direction.

Figure 10 (c) and (d) show the self-similar behaviour of the Q^- attached events extending beyond the buffer layer in all cases. The ratio $\Delta x/\Delta y$ has the highest probability at 2 and 1.5 for attached Q2 and Q4 events, respectively, while the ratio $\Delta x/\Delta z$ has the highest probability at 2.4 and 1.8. As a result, the length and width of tall-attached Q^- events follow well-defined linear laws as observed in Figure 10 (a) and (b) in this region.

In all cases, for tall-attached Q2 uv-structures,

$$\Delta x \approx 2\Delta y \approx 2.4\Delta z \tag{7}$$

while for tall-attached Q4 uv-structures,

$$\Delta x \approx 1.5\Delta y \approx 1.8\Delta z \tag{8}$$

In turbulent Poiseuille flow, Osawa [36] proved the self-similarity for Q^- (i.e. both Q2 and Q4 together) objects at $Re_\tau = 2003$ with $\Delta x \approx 2\Delta y \approx 2.5\Delta z$. This result agrees better with our result for Q2 events (Eq. 7), which makes sense since the percentage of identified tall-attached Q2 events is higher than Q4 as observed in Table II. Here, it is clear that self-similarity ratios in the logarithmic and outer regions are independent of the friction Reynolds number and the kind of channel flow (neutral, stratified Couette or neutral Poiseuille), at least in $Re_\tau \leq 2003$. Additionally, the use of a 26-directions connection algorithm does not seem to have an influence on the results. The above-mentioned authors used a 6-directions algorithm and their results agree well with this study.

As a result of the self-similarity, the volume of the boxes containing uv-structures can be expressed as $V^+_{box} = \Delta x^+ \times \Delta y^+ \times \Delta z^+ \propto (\Delta y^+)^3$ as shown in Figure 11 (top). The near-wall region ($\Delta y^+ < 100$) shows a poor agreement with the self-similar law as the height reduces. The region of minimum Δy^+ consists of attached Q4 events flattened against the wall due to their negative wall-normal velocity component. This fact was corroborated by plotting the box volume joint PDF of Q4 attached objects only, not shown here.

Although the volume of the boxes containing a uv-structure scales well with $(\Delta y^+)^3$, the volume of the uv-structures scales with $(\Delta y^+)^{2.45}$ as observed in Figure 11 (bottom). The volume of each structure is measured as the sum of the volume of all voxels contained in the structure. The difference in volume stems from the fact that the structures occupy a low percentage of the box volume in which they are contained. Del Álamo et al. [34] interpreted the scaling of the object volumes with their height as an estimate of their fractal dimension. In our case, the fractal dimension for attached Q^- events in all cases is 2.45. Lozano-Durán [30] found a similar fractal dimension in his study, concluding that the shapes of attached uv-structures resemble sponge-like objects formed by flakes.

IV. CONCLUSIONS

Using a database of several C-flows with active thermal flow, it is observed that the stratification at $\mathrm{Ri}_\tau \approx 3$ is enough to weaken the outer streamwise streaks, consequently vanishing the large-scale counter-rotating rolls, characteristic in neutral turbulent Couette channels. The

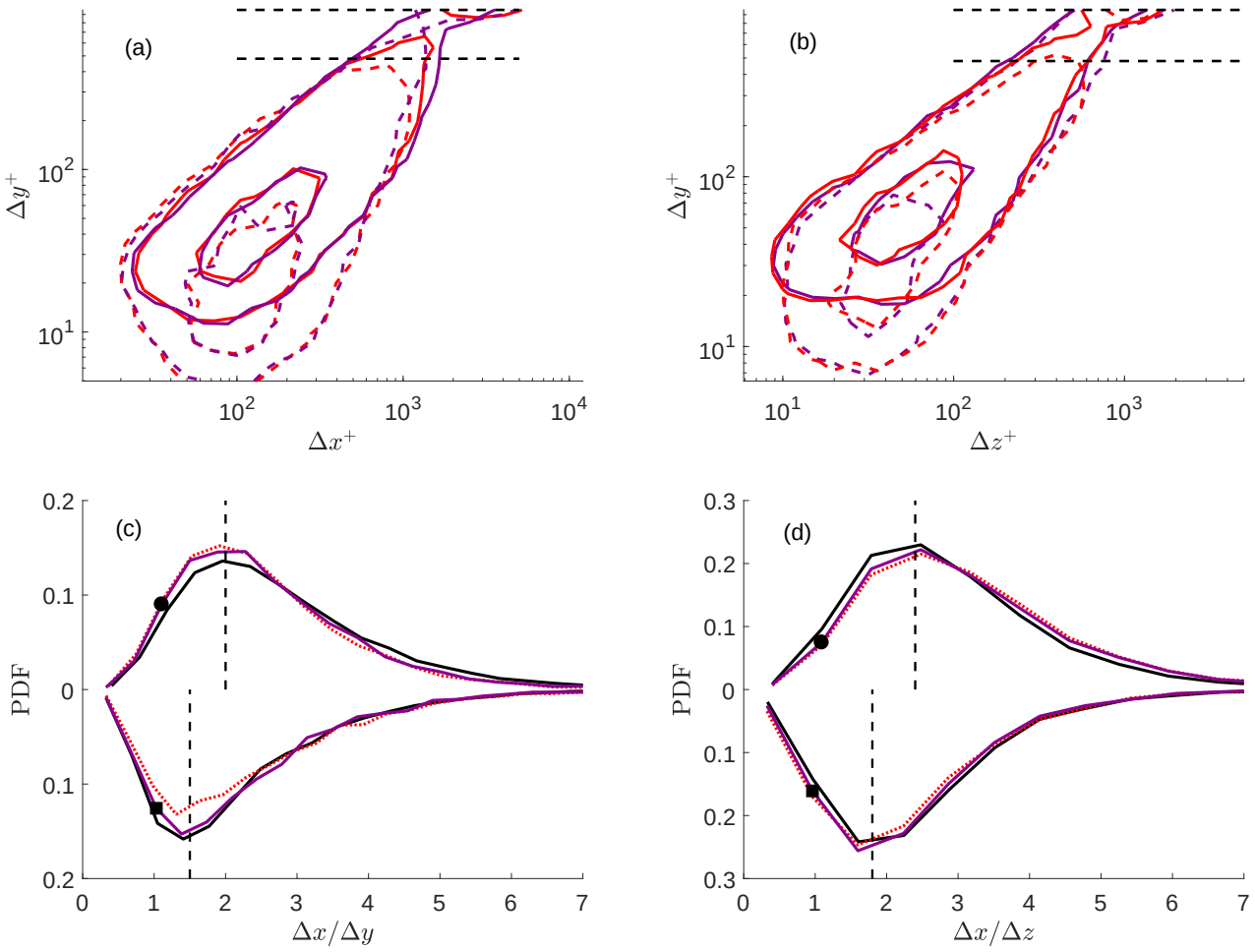

Figure 10: Colour online. Lines as in Table I. (a) Joint PDF of the length (Δx^+) and height (Δy^+) in wall units of boxes containing attached Q2 (solid lines) and attached Q4 (dashed lines) uv-structures. (b) Same as (a) for the width (Δz^+) and height (Δy^+) of the boxes. The contours present the 50% and 98% of the data. (c) PDF of the ratio $\Delta x/\Delta y$ of tall-attached Q2 (above $PDF = 0$) and Q4 (below). Signs as in Figure 7. (d) Same as in (c) for the ratio $\Delta x/\Delta z$. The horizontal dashed lines in (a) and (b) are Re_τ and $2Re_\tau$, respectively. The vertical lines in (c) are $\Delta x/\Delta y = [1.5, 2]$ and in (d) are $\Delta x/\Delta z = [1.8, 2.4]$.

weakening of the outer streaks is presumably caused by the well-known restriction on vertical motions imposed by the stratification, which at low stratification levels is only notorious above the buffer layer. It has been recently proven that such restriction causes the rupture of the self-sustaining mechanism between streaks and rolls at stratification levels similar to this study. Based on these facts, large-scale rolls will hardly appear in real-life Couette flows of air with a stable wall-normal gradient of temperature, as soon as Ri_τ passes a relatively low threshold.

Evaluating the coherent structures responsible for the momentum transfer (i.e. uv-structures) by filtering, the structures can be divided into attached and detached, depending on their distance to the nearest domain wall. As observed in previous studies of neutral channels, attached structures carry a great fraction of the total Reynolds stress, while detached structures are dissipative objects whose contribution cancels in average. This fact is kept under stratification, although the intensity of detached structures increases in the channel center. We focus on intense structures of negative Reynolds stress extending beyond the buffer layer; that is, tall-attached structures defining the bursting activity of ejections (Q2) and sweeps (Q4). The presence of streaks develops preferential locations for these structures in the spanwise direction. These locations match with the dimension of the rolls, showing a spatial relationship between streaks, rolls and bursting activity. The loss of the streaks due to stratification produces a disorganized scenario in terms of tall-attached that no longer supports the characteristic spatial organization of the rolls. Additionally, the average intensity of the ejections and sweeps is reduced.

Despite the intensity changes due to stratification, the

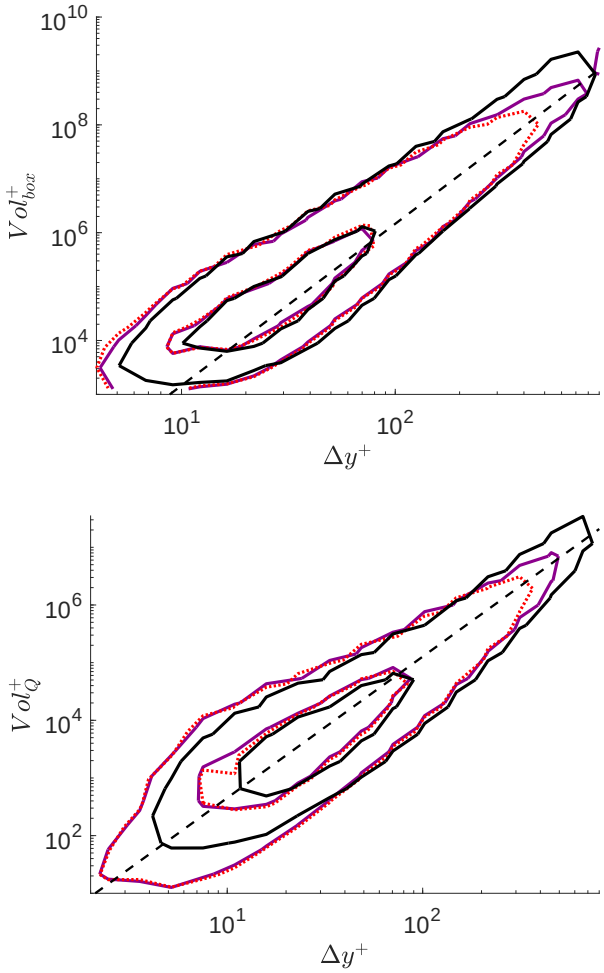

Figure 11: Colour online. Lines as in Table I. (Top) Joint PDF of the box volume and the height in wall units of attached Q^- events. The dashed line is $1.46\,(\Delta y^+)^3$. (Bottom) Same as in Top with the volume of the objects measured by voxels and their height in wall units. The dashed line is $1.6\,(\Delta y^+)^{2.45}$. In both figures, the contours contain 50% and 95% of the data.

geometry of the boxes containing tall-attached events is proven self-similar, showing the same linear scaling of their length and width as in neutral Couette and Poiseuille flows. Therefore, the volume of their boxes scale with their distance to the wall, which in attached events it is approximately Δy.

Observing the structure volume estimated as the sum of the volume of the structure voxels, all attached events scale well with $(\Delta y^+)^D$, being $D = 2.45$. This parameter is considered a rough fractal dimension of the structures, showing that attached structures resemble sponge-like objects formed by flakes.

ACKNOWLEDGMENTS

This work was supported by RTI2018-102256-B-I00 of MINECO/FEDER. The computations of the new simulations were made possible by a generous grant of computing time from the Barcelona Supercomputing Centre, reference AECT-2020-2-0005. FAA is partially funded by GVA/FEDER project ACIF2018.

[1] J. Kim, P. Moin, and R. Moser. Turbulence statistics in fully developed channels flows at low Reynolds numbers. *Journal of Fluid Mechanics*, 177:133–166, 1987.

[2] Sergio Hoyas and Javier Jiménez. Scaling of the velocity fluctuations in turbulent channels up to $Re_\tau = 2003$. *Physics of Fluids*, 18(1):011702, 2006.

[3] M. Bernardini, S. Pirozzoli, and P. Orlandi. Velocity statistics in turbulent channel flow up to $Re_\tau = 4000$. *Journal of Fluid Mechanics*, 758:327343, 2014.

[4] M. Lee and R. Moser. Direct numerical simulation of turbulent channel flow up to $Re_\tau \approx 5200$. *Journal of Fluid Mechanics*, 774:395–415, 2015.

[5] Yoshinobu Yamamoto and Yoshiyuki Tsuji. Numerical evidence of logarithmic regions in channel flow at $Re_\tau = 8000$. *Physical Review Fluids*, 3:012602(R), 2018.

[6] T. Tsukahara, H. Kawamura, and K. Shingai. DNS of turbulent Couette flow with emphasis on the large-scale structure in the core region. *Journal of Turbulence*, 7:1–16, 2006.

[7] V. Avsarkisov, S. Hoyas, M. Oberlack, and J.P. García-Galache. Turbulent plane Couette flow at moderately high Reynolds number. *Journal of Fluid Mechanics*, 751:R1, 2014.

[8] S. Pirozzoli, M. Bernardini, and P. Orlandi. Turbulence statistics in Couette flow at high Reynolds number. *Journal of Fluid Mechanics*, 758:323–343, 2014.

[9] N. Tillmark. *Experiments on transition and turbulence in plane Couette flow.* PhD thesis, KTH, Royal Institute of Technology, 1995.

[10] O. Kitoh, K. Nakabyashi, and F. Nishimura. Experimen-

tal study on mean velocity and turbulence characteristics of plane Couette flow: Low-Reynolds-number effects and large longitudinal vortical structure. *Journal of Fluid Mechanics*, 539:199–227, 2005.

[11] K. Bech, N. Tillmark, P. Alfredsson, and H. Andersson. An investigation of turbulent plane Couette flow at low Reynolds numbers. *Journal of Fluid Mechanics*, 286:291325., 1995.

[12] M. Lee and R. Moser. Extreme-scale motions in turbulent plane Couette flows. *Journal of Fluid Mechanics*, 842:128–145, 2018.

[13] M. Atzori, R. Vinuesa, A. Lozano-Durán and P. Schlatter. Characterization of turbulent coherent structures in square duct flow, *Journal of Physics*: Conference Series 1001 (1), 012008, (2018).

[14] S. Kraheberger, S. Hoyas, and M. Oberlack. DNS of a turbulent Couette flow at constant wall transpiration up to $Re_\tau = 1000$. *Journal of Fluid Mechanics*, 835:421–443, 2018.

[15] Sergio Gandía-Barberá, Sergio Hoyas, Martin Oberlack and Stefanie Kraheberger. The link between the Reynolds shear stress and the large structures of turbulent Couette-Poiseuille flow. *Physics of Fluids*, 30, 041702, 2018.

[16] Alcántara-Ávila, F. and Gandía Barberá and Hoyas, S. Evidences of persisting thermal structures in Couette flows. *International Journal of Heat and Fluid Flow*, 76, 287-295, 2019.

[17] RLF Oglethorpe, CP Caulfield, and AW Woods. Spontaneous layering in stratified turbulent TaylorCouette flow *, J. Fluid Mech.* (2013), vol. 721, R3

[18] T. S. Eaves and C. P. Caulfield. Disruption of SSP/VWI states by a stable stratification. *J. Fluid Mech.*, 784, 548-564, 2015.

[19] Enrico Deusebio, C. P. Caulfield and J. R. Taylor. The intermittency boundary in stratified plane Couette flow. *Journal of Fluid Mechanics*, 781:298-329, 2015.

[20] R.K.Smith, G. a Roff, and N. Crook. The Morning Glory: An extraordinary atmospheric undular bore. *Quarterly Journal of the Royal Meteorological Society*, 108, 937-956, 1982.

[21] V. Avsarkisov, B. Strelnikov and E. Becker. Analysis of the vertical spectra of density fluctuation variance in the strongly stratified turbulence. *Proceedings of the 11th International Symposium on Turbulence and Shear Flow Phenomena (TSFP 11)*, 1-5, 2019.

[22] S. K. Lele. Compact finite difference schemes with spectral-like resolution. *Journal of Computational Physics*, 103(1):16–42, 1992.

[23] Philippe R Spalart, Robert D Moser, and Michael M Rogers. Spectral methods for the Navier-Stokes equations with one infinite and two periodic directions. *Journal of Computational Physics*, 96(2):297–324, 1991.

[24] S. Hoyas and J. Jiménez. Reynolds number effects on the Reynolds-stress budgets in turbulent channels. *Physics of Fluids*, 20(10):101511, 2008.

[25] V. Avsarkisov, M. Oberlack, and S. Hoyas. New scaling laws for turbulent Poiseuille flow with wall transpiration. *Journal of Fluid Mechanics*, 746:99-122, 2014.

[26] F. Lluesma-Rodríguez, S. Hoyas, and MJ Peréz-Quiles. Influence of the computational domain on DNS of turbulent heat transfer up to $Re_\tau = 2000$ for $Pr = 0.71$. *International Journal of Heat and Mass Transfer*, 122:983–992, 2018.

[27] M García-Villalba, and Juan C. Del Álamo, Turbulence modification by stable stratification in channel flow. *Physics of Fluids*, 23 045104, 2011.

[28] R. L. Panton. Overview of the self-sustaining mechanisms of wall turbulence. *Prog. Aerosp. Sci.*, 37: 341-383, 2001.

[29] H. J. Bae, M. P. Encinar and A. Lozano-Durán. Causal analysis of self-sustaining processes in the logarithmic layer of wall-bounded turbulence. *Journal of Physics: Conference Series, IOP Publishing*, 2018, 1001, 012013.

[30] A. Lozano-Durán, O. Flores and J. Jiménez. The three-dimensional structure of momentum transfer in turbulent channels. *Journal of Fluid Mechanics*, 694: 100-130, 2012.

[31] J. Jiménez Coherent structures in wall-bounded turbulence. *Journal of Fluid Mechanics*, 842, P1, 2018.

[32] A. Lozano-Durán and J. Jiménez Time-resolved evolution of coherent structures in turbulent channels: characterization of eddies and cascades. *Journal of Fluid Mechanics*, 759, 432-471, 2014.

[33] A. Lozano-Durán and Borrell, Guillem. Algorithm 964: An Efficient Algorithm to Compute the Genus of Discrete Surfaces and Applications to Turbulent Flows. *Association for Computing Machinery*, 42, 4, July 2016.

[34] J. C. Del Álamo, J. Jiménez, P. Zandonade and R.D. Moser Self-similar vortex clusters in the turbulent logarithmic region. *Journal of Fluid Mechanics*, 561: 329-358, 2006.

[35] R Nagaosa and R.A. Handler Statistical analysis of coherent vortices near a free surface in a fully developed turbulence. *Physics of Fluids*, 15, 375-394, 2003.

[36] K. Osawa and J. Jiménez. Intense structures of different momentum fluxes in turbulent channels. *Phys. Rev. Fluids*, 3, 084603, 2018.

[37] Yoon M., Hwang, J., Yang, J. and Sung, H.J. Wall-attached structures of streamwise velocity fluctuations in an adverse-pressure-gradient turbulent boundary layer. *Journal of Fluid Mechanics*, 885: A12, 2020.